USGS
science for a changing world

Ground Deformation and Gravity for Volcano Monitoring

Chapter D of
Recommended Capabilities and Instrumentation for Volcano Monitoring in the United States

Scientific Investigations Report 2024–5062

U.S. Department of the Interior
U.S. Geological Survey

Cover. U.S. Geological Survey scientist A. Ellis installing a temporary Global Navigation Satellite System station south of the summit of Kīlauea, Hawai'i. This station is part of a network of stations measured annually. The long profile of Mauna Loa is prominent in the background. Photograph by D. Phillips, U.S. Geological Survey, May 2024. Background image shows a typical view of the 2008–2018 lava lake in the Overlook crater within Halema'uma'u, Kīlauea. Photograph taken from a helicopter by Tim Orr, U.S. Geological Survey, on August 16, 2013.

Ground Deformation and Gravity for Volcano Monitoring

By Emily K. Montgomery-Brown, Kyle R. Anderson, Ingrid A. Johanson, Michael P. Poland, and Ashton F. Flinders

Chapter D of
Recommended Capabilities and Instrumentation for Volcano Monitoring in the United States

Edited by Ashton F. Flinders, Jacob B. Lowenstern, Michelle L. Coombs, and Michael P. Poland

Scientific Investigations Report 2024–5062

U.S. Department of the Interior
U.S. Geological Survey

U.S. Geological Survey, Reston, Virginia: 2024

Suggested citation:
Montgomery-Brown, E.K., Anderson, K.R., Johanson, I.A., Poland, M.P., and Flinders, A.F., 2024, Ground deformation and gravity for volcano monitoring, chap. D *of* Flinders, A.F., Lowenstern, J.B., Coombs, M.L., and Poland, M.P., eds., Recommended capabilities and instrumentation for volcano monitoring in the United States: U.S. Geological Survey Scientific Investigations Report 2024–5062–D, 11 p., https://doi.org/10.3133/sir20245062D.

ISSN 2328-031X (print)
ISSN 2328-0328 (online)

Contents

Figures

Sidebar

Conversion Factors

International System of Units to U.S. customary units

Multiply	By	To obtain
	Length	
millimeter (mm)	0.03937	inch (in.)
meter (m)	3.281	foot (ft)
kilometer (km)	0.6214	mile (mi)
meter (m)	1.094	yard (yd)

Abbreviations

EDM	electronic distance measurement
GNSS	Global Navigation Satellite System
InSAR	interferometric synthetic aperture radar

Recommended Capabilities and Instrumentation for U.S. Volcano Monitoring
Edited by A.F. Flinders, J.B. Lowenstern, M.L. Coombs, and M.P. Poland
Scientific Investigations Report 2024–5062

Chapter D

Ground Deformation and Gravity for Volcano Monitoring

By Emily K. Montgomery-Brown, Kyle R. Anderson, Ingrid A. Johanson, Michael P. Poland, and Ashton F. Flinders

Introduction

When magma accumulates or migrates, it can cause pressurization and related ground deformation. Characterization of surface deformation provides important constraints on the potential for future volcanic activity, especially in combination with seismic activity, gas emissions, and other indicators. A wide variety of techniques and instrument types have been applied to the study of ground deformation at volcanoes (sidebar ,p. 2; Dzurisin, 2000, 2003, 2007). Geodetic instruments include continuously recording Global Navigation Satellite System (GNSS; of which the United States' Global Positioning System is one example) stations (fig. D1), borehole tiltmeters, and interferometric synthetic aperture radar (InSAR) measurements (from satellites, occupied and unoccupied aircraft systems, and ground-based sensors). Additional geodetic measurements like continuous- and survey-mode gravity (fig. D2) can contribute substantially to interpreting these data. Borehole strainmeters (see chapter K, this volume, by Hurwitz and Lowenstern, 2024) also have outstanding utility for monitoring deformation, although because of cost and permitting challenges, we do not include them as part of standard volcano monitoring networks for U.S. volcanoes. Still other techniques like light detection and ranging (lidar), structure from motion, and optical satellite data can be used to derive gross topographic changes, which can be used to map volcanic deposits, infer eruption rates, and gain insights into the source processes associated with eruptive activity (see chapter G, this volume, on tracking surface changes caused by volcanic activity; Orr and others, 2024).

Figure D1. Photograph showing a U.S. Geological Survey Hawaiian Volcano Observatory geophysicist downloading data from the Global Navigation Satellite System (GNSS) station PUL2 along the middle East Rift Zone of Kīlauea, Hawai'i. This semi-permanent station was deployed during the 2018 eruption to help monitor ongoing deformation from Kīlauea's East Rift Zone and from a magnitude 6.9 earthquake. Photograph by P. Dotray, U.S. Geological Survey, September 10, 2019.

Figure D2. Photograph showing U.S. Geological Survey geophysicist measuring gravity at a station on the rim of Mount St. Helens, Washington. This station, NWDO, is northwest of the 2004–08 lava dome and part of the Mount St. Helens campaign gravity network. Positive residual gravity anomalies from this and five other stations indicated a net subsurface mass increase on the 2004–08 lava dome from 2010 to 2016. Spirit Lake can be seen in the middle ground, and Mount Rainier, Washington, in the background. Photograph by M. Poland, U.S. Geological Survey, August 17, 2010.

Sidebar—Description of geodetic techniques

[km, kilometer; m, meter]

Geodetic Technique	Description	Utility
Global Navigation Satellite Systems (GNSS) 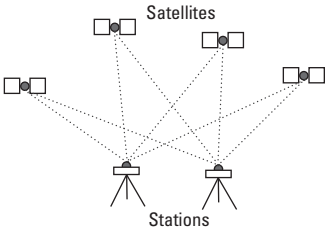	Antenna and receiver packages are installed permanently or temporarily over ground markers to record orbiting satellite messages that are used to compute precise positions.	Good temporal resolution, three-dimensional motions, and potential for real-time monitoring. Spatial coverage may be limited by permitting and financial considerations.
Interferometric synthetic aperture radar (InSAR) 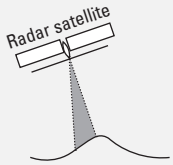	Interference between paired images from a radar satellite taken at different times from slightly different places is used to determine the deformation that occurred between image acquisitions.	Good spatial coverage over light vegetation. Data availability depends on satellite orbital parameters and space agency priorities.
Electronic distance measurement (EDM) 	Horizontal laser distance measurements are compared to determine horizontal deformation changes. Measurements are commonly made at two optical frequencies to correct for atmospheric interference.	Labor- and time-intensive measurement practices, meaning that EDM is commonly limited to smaller networks and infrequent data collection.
Leveling 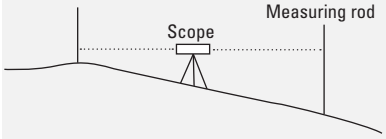	Measurements of vertical elevation along profile lines that can be compared to determine vertical deformation changes.	Highly accurate. Labor- and time-intensive measurement practices, meaning that leveling is commonly limited to smaller networks and infrequent data collection.
Tiltmeter 	Electronic measurement of ground tilt (like a carpenter's level).	Capable of high-frequency (~1 minute) temporal sampling, making it useful for real-time monitoring; particularly sensitive to shallow magma sources. Lowest noise data require expensive boreholes; platform installations offer a noisier alternative. Can be subject to anomalous signals caused by daily thermal signals, rainfall effects, and so on.
Microgravity changes 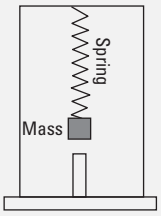	A highly accurate gravimeter measures changes in gravity caused by subsurface mass changes.	Instruments are expensive and surveys are time intensive. Measurements are most sensitive to shallow (<3 km) gravity sources.
Borehole strainmeter 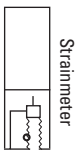	An instrument coupled to rock inside a relatively deep (200–250 m) borehole; measures crustal strain.	Capable of high-frequency temporal sampling (1–2 minutes). Sensitive to small changes. Expensive to drill a borehole.

Experience has shown that no single geodetic monitoring technique is adequate to detect and track the entire range of ground-motion patterns that occur at volcanoes, primarily because of the temporal and spatial diversity of volcano deformation (fig. D3). Similarly, the magnitude of surface deformation varies widely. Geodetic monitoring strategies should therefore include multiple techniques and instrument types to cover a wide range of spatial and temporal scales.

In identifying recommendations for geodetic instrumentation for volcano monitoring networks, we attempted to maximize the diversity of instrument types to measure the full range of deformation signals and minimize their expense and number; thus, we do not include several well-known deformation-monitoring techniques in our recommendations. Extensometers, for example, measure strains over distances of a few meters and have an excellent record of success in detecting changes in preeruptive localized ground motion across existing cracks, including at Mount St. Helens, Washington (Iwatsubo and others, 1992), and Piton de la Fournaise, Réunion Island (Peltier and others, 2006). Despite being relatively inexpensive, extensometers are best used primarily when localized ground displacements (for example, ground cracks) need to be tracked, and are not necessary at all volcanoes.

In considering volcano deformation monitoring strategies, two complicating factors are deserving of special attention. First, not all deformation is driven by subsurface magmatic activity—for example, at many large stratovolcanoes (for example, Mount Rainier), flank collapses and landslides are significant geologic hazards (Reid and others, 2001) that may occur even in the absence of magmatic activity. Monitoring the stability of volcanoes is thus another critical application of geodetic monitoring networks to inform hazard assessment. One of the most famous examples of edifice instability is the large flank collapse that initiated the May 18, 1980, eruption of Mount St. Helens. Deformation monitoring had detected a bulge on the north flank of the mountain in April 1980 that was expanding by several meters per day (Lipman and others, 1981). Given that flank collapses can happen at any time during a period of volcanic unrest (or even outside a period of unrest), the capability to assess edifice stability is critical.

Second, although volcanoes are commonly treated as idealized structures that erupt from single points, like central-vent stratovolcanoes, many are characterized by long rift zones from which eruptions may originate, and distributed volcanic fields are characterized by broadly spaced vents. For example, linear dikes are common at Kīlauea, Mauna Loa, and between Mount Shasta and Medicine Lake in California. At Kīlauea, one of these linear dikes emerged more than 40 kilometers (km) away from the summit of the volcano during the lower East Rift Zone eruption in 2018. Other volcanic fields, like Lassen volcanic center, California, or the San Francisco Volcanic Field, Arizona, have many small vents spread over a wide area. Although the instrumentation guidelines presented in this chapter remain phrased for central-vent volcanoes, they should be modified as needed in the context of the eruptive characteristics of each individual volcanic system.

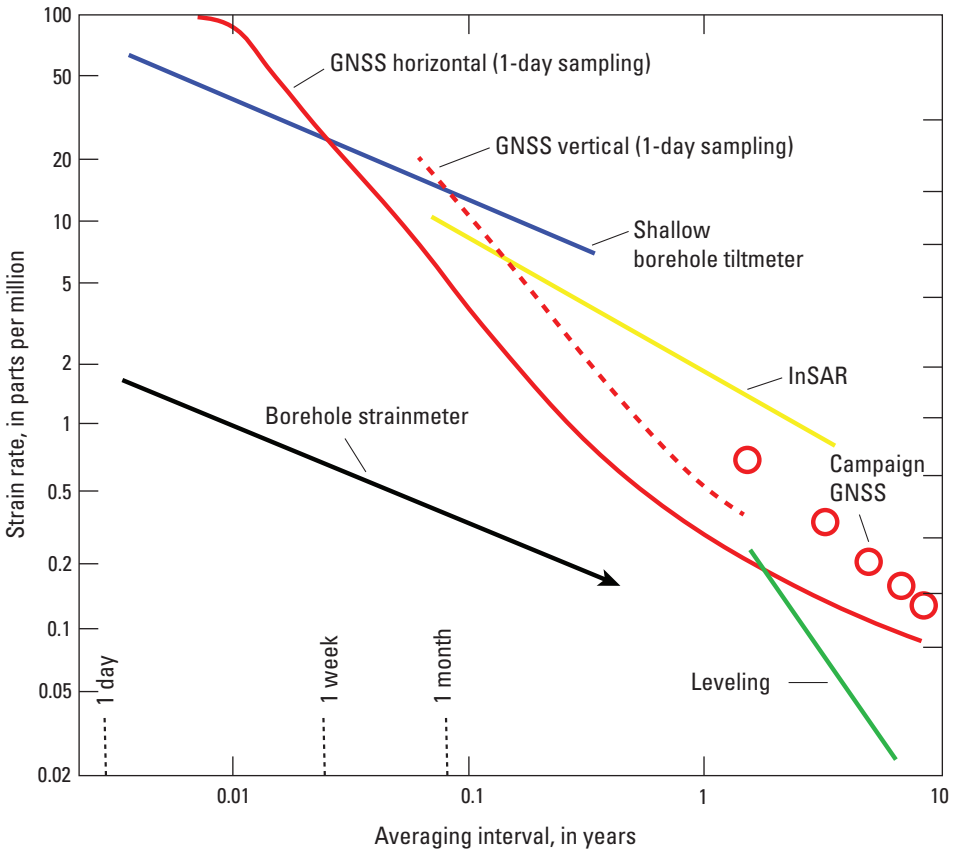

Figure D3. Graph showing strain rate detection limits versus averaging interval for typical volcano geodetic monitoring techniques. Strains for permanent Global Navigation Satellite System (GNSS) stations and interferometric synthetic aperture radar (InSAR) pixels are calculated assuming stations are 8 kilometers apart. Circles represent campaign GNSS measurements at longer time intervals. Note that borehole strainmeters provide the best measurements over timescales of minutes to days, whereas campaign GNSS, leveling, and InSAR provide the best measurements over months to years. Thus, multiple types of instrumentation are recommended to provide optimal geodetic observations over both space and time. Modified from Dzurisin (2007).

Spatial analysis of geodetic network coverage could help to ensure adequate instrumentation in areas where volcanism can occur over a broad area as opposed to a central vent. As an example, consider the adjacent volcanoes Mount Shasta and Medicine Lake. If station locations are chosen based only on the distance from the centers of the volcanoes, then any geodetic anomalies between the two volcanoes—an area of potential volcanism as indicated by the presence of volcanic features—may remain undetected by ground-based instrumentation. The spatial analysis is accomplished via a grid of pressure point sources (Mogi, 1958) evenly distributed across the map area, at a depth of 5 km in this example (fig. D4). Each source is inflated until predicted deformations exceed the GNSS white noise uncertainty estimates at one site (Langbein, 2017; Murray and Svarc, 2017). This volume of detectable magma provides a measure of the quality of the coverage (fig. D4). The results indicate that, as of 2022, there is a large area between Mount Shasta and Medicine Lake volcano with existing mapped dikes in which a substantial amount of magma could intrude without being detected geodetically. Applying this style of analysis to individual volcanic systems can provide a guide for designing network geometry given the expected locations of future eruptions.

Recommended Capabilities

The three capabilities, increasingly relevant at higher threat volcanoes, recommended here for deformation monitoring networks are (1) detection of changes in deformation patterns, potentially in near-real time, (2) if deformation is detected, then localization of subsurface source(s) of deformation in three dimensions and estimation of its (their) magnitude and geometry, and (3) if deformation is detected, recognition of magmatic versus nonmagmatic deformation. Capabilities 2 and 3 are intimately linked because the volume and depth of a source must first be estimated to infer its origin, but we describe these capabilities separately for clarity and provide justification based on examples from volcanoes around the world.

We make recommendations for specific numbers of instruments to enable each capability. The GNSS instrumentation recommendations are partly based on numerical simulations of hypothetical surface-deformation patterns. Given the diversity of volcano type, size, eruptive behavior, local geography, accessibility, and environment, the instrument mix and deployment strategy should be customized to each volcano. Accordingly, we give ranges of instrument numbers but, as

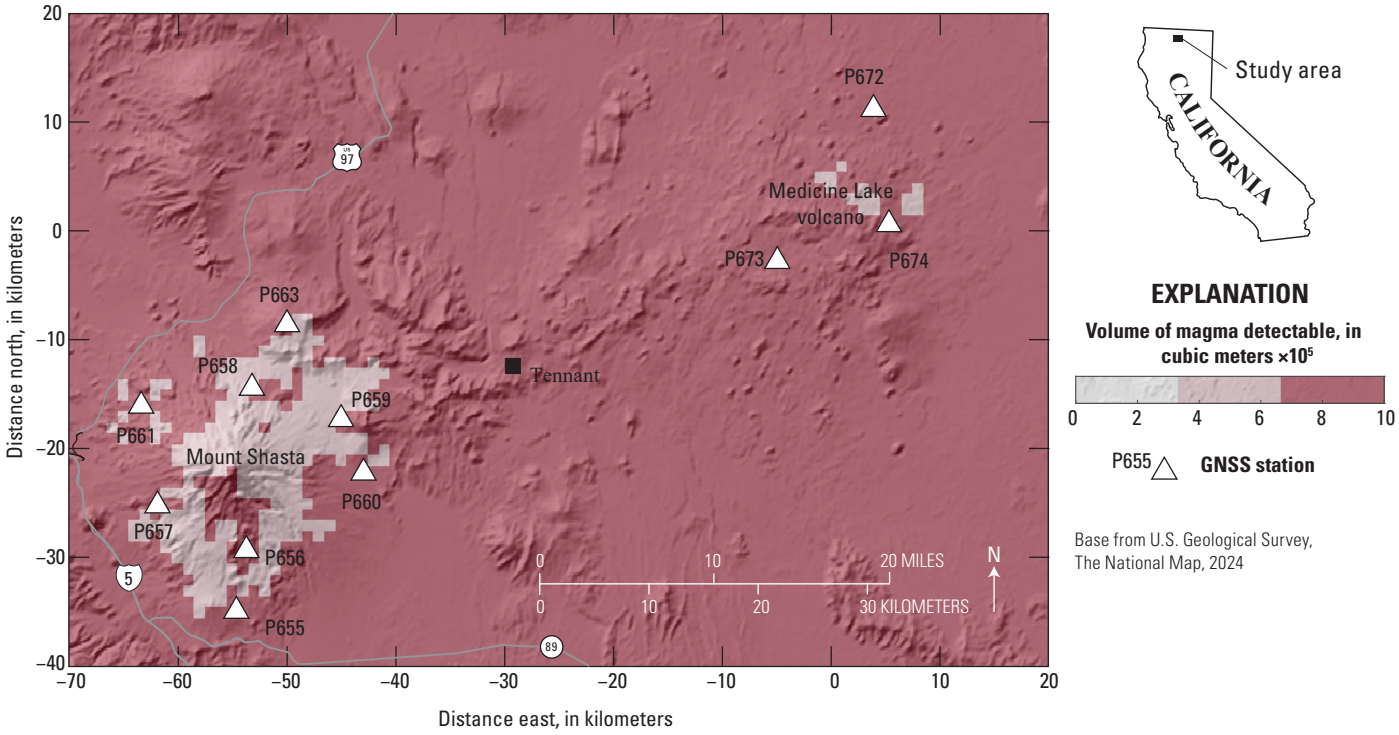

Figure D4. Map showing the amount of magma detectable by the current Global Navigation Satellite System (GNSS) networks at Mount Shasta and Medicine Lake volcano, California. Acceptable coverage is observed at the volcanic centers; however, minimal coverage is present in the area between them where evidence of past eruptions exists. The darkest areas indicate regions where more than 0.001 cubic kilometer ($1x10^6$ cubic meters) of magma could intrude undetected by the GNSS network.

discussed in this volume's introduction (Flinders and others, 2024), there are financial, practical, and scientific considerations that will ultimately govern the monitoring strategies that can be deployed at any specific volcano.

Detect Changes in Surface Deformation Patterns

Although detecting spatial and temporal changes in surface deformation may be the most important capability of a geodetic monitoring network, it is challenging because of the wide range of time and length scales over which these changes can take place. In terms of timing, precursory deformation was detected only 30 minutes before the eruption of Hekla in Iceland in 1991 (Linde and others, 1993), several hours before an eruption at Mount Etna in Italy in 2002 (Aloisi and others, 2003), and 7 minutes before the phreatic eruption at Ontake in Japan in 2016 (Yamaoka and others, 2016). Deformation measurements at Mount St. Helens contributed to successful predictions days to weeks before more than a dozen dome-building eruptions during 1980–86 (Swanson and others, 1983; Chadwick and others, 1988; Chadwick and Swanson, 1989). At the long end of the range, anomalous surface deformation can extend for months to years. For example, at Augustine Volcano, Alaska, deformation was recognized several months before the onset of eruptive activity there in 2006 (Cervelli and others, 2006), and InSAR-detected deformation at Three Sisters, Oregon (Wicks and others, 2002), could represent an example of decades-long intrusive deformation that may never result in an eruption. An eruption did occur at Rabaul, Papua New Guinea, after decades of deformation (Robertson and Kilburn, 2016). The capability to detect short- and long-term changes in the deformation field is therefore critical for characterizing stable magma systems and more rapid changes.

Spatial scales of deformation can be similarly diverse. Highly localized deformation has been detected prior to small phreatic explosions in Japan (Kobayashi, 2018), whereas surface displacements prior to the 2009 eruption of Redoubt Volcano, Alaska, were detected at a GNSS site nearly 30 km from the volcano (Grapenthin and others, 2013). Broad regions of gentle surface uplift—centimeters of ground motion spread over tens of kilometers—have been associated with magma accumulation in several locations, including multiple volcanoes in the central Andes of South America (Pritchard and Simons, 2004).

Instrumentation

GNSS receivers and borehole tiltmeters currently can provide the required near-real-time data but should have a latency of no more than a few minutes. Whereas GNSS can detect near-real-time deformation, real-time solutions can be subject to substantial noise sources. Tilt is especially sensitive for detecting changes over minutes to hours in shallow magma sources, and arrays of borehole tiltmeters have been used independently of other data types to model source depths and volume changes at Kīlauea (Miklius and Cervelli, 2003; Anderson and others, 2015). Continuous gravimeter and strainmeter stations can also provide sensitive real-time ground-displacement measurements, although gravimeters must be co-located with a continuous-mode GNSS station for elevation control. High-rate GNSS should also be exploited as a tool for detecting rapid transient deformation and enabling measurements of three-dimensional position changes. These instruments complement each other, providing different sensitivities and capabilities (table D1) that can be used to measure a range of geodetic changes at volcanoes. For example, borehole tilt is well suited to detect short-term transient deformation, like dike intrusion, whereas GNSS is more stable over longer time periods and thus better for tracking signals like slow inflation. Episodic InSAR measurements and GNSS and gravity surveys would ideally be performed, if practical, to provide longer term measurements with higher spatial resolution than is possible with continuous-mode stations. InSAR is especially useful for detecting and characterizing flank stability (for example, Schaefer and others, 2019).

Recommendations

For level 1 volcanoes, we recommend establishing a baseline monitoring network with the purpose of understanding background deformation characteristics and tectonic influences. This baseline can then be used for comparison in the future if continuous geodetic monitoring becomes necessary. Baseline monitoring can be done primarily by InSAR with an annual or several-year cadence and prioritize development of automated processing and detection algorithms. Baseline GNSS and gravity survey networks would ideally be established and remeasured occasionally (5–10 years) with the goal of understanding background local and tectonic deformation.

At level 2 volcanoes, the goal is to detect long-term deformation changes. Thus, campaign GNSS data should be collected every 1–5 years to supplement automated InSAR monitoring and allow for repeat gravity surveys. One continuous-mode GNSS station is recommended within a few kilometers of the most likely vent location (distance dependent on the size of the volcano).

For level 3 volcanoes, spatial and temporal scales of deformation can vary widely, requiring both increased spatial density and real- or near-real-time data with a goal of detecting rapid changes in the deformation field detected within a few days (depending on the magnitude and style of the signal). Two or three continuous-mode GNSS stations within 5–10 km of the deforming source are recommended, and one or more stations farther afield are recommended to provide a stable reference outside the deforming region. A borehole tiltmeter is also recommended if the magma system is shallow and susceptible to signals in the detectable range of tiltmeters. Gravity surveys should be repeated as practical every few years. Automated InSAR processing and analysis should be scrutinized annually, or more often if deformation is detected.

Finally, at level 4 volcanoes, deformation changes would ideally be detected with a lower latency of no more than a few hours, depending on signal magnitude and pattern, and increased station density to cover the possible deforming regions. Five to

eight continuous-mode GNSS stations are recommended for detecting deformation changes. If conditions are appropriate, two to three borehole tiltmeters would be placed near the deformation source. One continuous gravimeter would be placed near the volcano, as close as possible to any likely sources of mass change (because the strength of any gravity signal will diminish rapidly with distance), co-located with a continuous-mode GNSS station for elevation control. The volcano would ideally receive regular tasking by InSAR-capable satellites, with interferograms generated across weeks to months as conditions warrant.

Locate Geodetic Sources and Estimate Source Magnitude and Geometry

Another primary goal of deformation monitoring at active volcanoes is to map the geometry, strength (generally expressed as change in volume), and three-dimensional position of magma bodies. Is an intrusion growing? Where (and how deep) is it? Can we map its movement over time? Source volume change and location cannot be uniquely determined if the spatial resolution of deformation measurements is too low. For example, Delaney and McTigue (1994) showed that volume-change estimates depend heavily on reservoir geometry, but campaign measurements at deforming volcanoes can commonly be fit equally well by multiple deformation source geometries (Dzurisin and others, 2002; Fournier and Freymueller, 2008)—such as point sources of volume change (Mogi, 1958) and horizontal opening-mode dislocations that approximate sills (Okada, 1985). Volume changes calculated from the different geometries can vary by 30 percent (Dzurisin and others, 2002). Source depth also depends on geometry, and this trade-off can result in uncertainty if data coverage is insufficient; for example, sources that are shallow and weak can produce deformation magnitudes that are similar to sources that are deep and strong. Because different source geometries produce different patterns of horizontal and vertical surface deformation (for example, Dieterich and Decker, 1975), any geodetic monitoring network would ideally have the capability of measuring different components and spatial scales of ground displacements to distinguish among competing models.

Estimates of source strength are important to assessments of future activity, especially at restless or active volcanoes. For example, at Soufrière Hills volcano, Montserrat, GNSS measurements detected time-varying behavior of a deformation source 5–6 km beneath the volcano (Wadge and others, 2006). During eruptive periods, they showed that the reservoir (source) contracted as magma withdrawal exceeded supply from deeper regions. During eruptive pauses, the reservoir inflated as magma accumulated. Rates of volume change are therefore useful as an indicator of the likely future course of an eruption. Magma accumulation beneath active volcanoes can be steady or episodic, and long-term records such as those at Kīlauea and Mauna Loa are especially useful. Xue and Freymueller (2020) constructed an approximately 25-year record of magma accumulation for three Aleutian Arc volcanoes using a fusion of campaign and continuous GNSS data with InSAR; they found a variety of timescales for episodic and near-continuous magma accumulation.

The ability to distinguish between one versus multiple deformation sources is also critical for inferring source location, depth, and strength. For example, surface deformation at Mauna Loa has been modeled as caused by a combination of two sources (a point source and a dike), resulting in a complex deformation field (Amelung and others, 2007; Varugu and Amelung, 2021). Separating these two sources was critical in assessing the unrest leading up to the 2022 eruption of Mauna Loa and seeing the shallowing of the dike. If the deformation-monitoring network contains too few stations or is not designed to distinguish between the effects of these two competing sources, interpretations of surface-deformation data would be unreliable and could lead to incorrect interpretations of volcanic unrest. At Mount Okmok, Alaska, for example, Xue and others (2020) found that InSAR and GNSS displacements gave different estimates of the magma system geometry owing to the different spatial sampling of the data, although both datasets could be satisfied by a combination of a point source and a shallow sill-like source.

Instrumentation

For the best sensitivity to source location, geometry, and strength, deformation should be measured over a range of distances from the source. These measurements can be done in near-real time with a network of continuous-mode GNSS instruments and borehole tiltmeters, or over longer time scales using InSAR and (or) GNSS surveys. Both strategies should be used because InSAR measurements and GNSS surveys provide the densest spatial resolution, whereas borehole tilt and continuous-mode GNSS provide the densest temporal resolution. InSAR and GNSS also have different sensitivities to nonvolcanic deformation sources (see following “Recommendations” section), which can bias estimates of source location and geometry.

To formalize a recommendation for numbers of near-real-time continuous-mode GNSS instruments, we performed numerical simulations of the sensitivity of the density of continuous-mode GNSS stations to a buried inflation source (fig. D5). In our hypothetical scenario, we assumed a source at 2.5-km depth, which is typical of the shallowest magma-accumulation zones at several volcanoes (Brandsdóttir and others, 1997; Iwashita and others, 2005; Pagli and others, 2006; Yun and others, 2006). Synthetic three-component surface displacements were forward-calculated for a point-source model (Mogi, 1958), assuming a modest volumetric inflation of 0.001 cubic kilometers. Gaussian random noise was added to the synthetic data by assuming a standard deviation of 2 millimeters (mm) in the horizontal components and of 6 mm in the vertical component (typical of continuous-mode GNSS data).

We used a Monte Carlo algorithm to run multiple simulations with different station distributions. A GNSS network was constructed by randomly locating stations around the volcanic edifice, with 95 percent of stations within 11 km of the volcano’s summit (beneath which the source is located) and a reference station 30 km away. A total of 1,000 simulations were performed for a given number of stations, with each simulation using a unique station distribution. The synthetic data were inverted

using a nonlinear minimization algorithm to solve for volumetric inflation, source depth, and location.

The uncertainty in model parameters (volume change and source depth) as a function of number of stations is plotted in figure D5. Resolution of source (the χ^2 parameter is a representation of the fitness of all combined model parameters—depth, location, and volume change) improves as the number of stations increases. For example, the uncertainty in source depth for a network of four stations is about ±2.5 km, indicating that the source could statistically reside anywhere from 0 to 5 km of the surface (given an actual source depth of 2.5 km). However, the uncertainty decreases to about ±1 km with a network of more than 15 stations. Volume-change uncertainty was similarly affected by the number of stations.

Recommendations

Given the relatively low threat level of levels 1 and 2 volcanoes, we do not recommend additional geodetic equipment for this capability in the absence of unrest. At level 3 volcanoes, it becomes more important to locate and estimate volume change within a subsurface deformation source. Five to 10 high-quality continuous-mode GNSS stations are recommended, of which four should be within 5 km of the deforming source and one outside the area of expected surface deformation (to provide a stable reference). In addition, two to four borehole tiltmeters placed within 5–10 km of the deforming source are recommended if the source is shallow and susceptible to deformation in the range measurable by tiltmeters. InSAR data would ideally be acquired and scrutinized at least on an annual basis, augmented by GNSS surveys every several years to fill in gaps not covered by the continuous GNSS network. Finally, we recommend a baseline gravity survey for reference if a potential magmatic intrusion is identified. At level 4 volcanoes, we seek to provide robust constraints on the location of, and volume change within, any subsurface deformation source. To achieve that end, we recommend 16 to 20 continuous-mode GNSS stations, of which at least eight are within 5–10 km of the deforming source and two are outside the area of expected surface deformation (to provide a stable reference for high-rate positioning, and to help distinguish volcanic and nonvolcanic deformation). In addition, if the source is appropriate, between four to six borehole tiltmeters would be placed within 5–10 km of the deforming source. Annual (summer to summer) InSAR measurements would be complemented with frequent summertime views, dependent on satellite cadence, at volcanoes where snow interferes with data quality. At snow-free volcanoes, InSAR images would ideally be compiled as frequently as is practical. Campaign GNSS surveys would be repeated every few years (if practical), particularly at those volcanoes where InSAR measurements are challenged by environmental conditions and where continuous-mode GNSS stations have detected anomalous surface deformation. One continuous gravimeter would ideally be placed near the volcano if conditions are appropriate. It should be installed as close as possible to any likely sources of mass change (because the strength of any gravity signal diminishes rapidly with distance) and be co-located with a continuous-mode GNSS station for elevation control. Repeat gravity surveys should cover the deforming area.

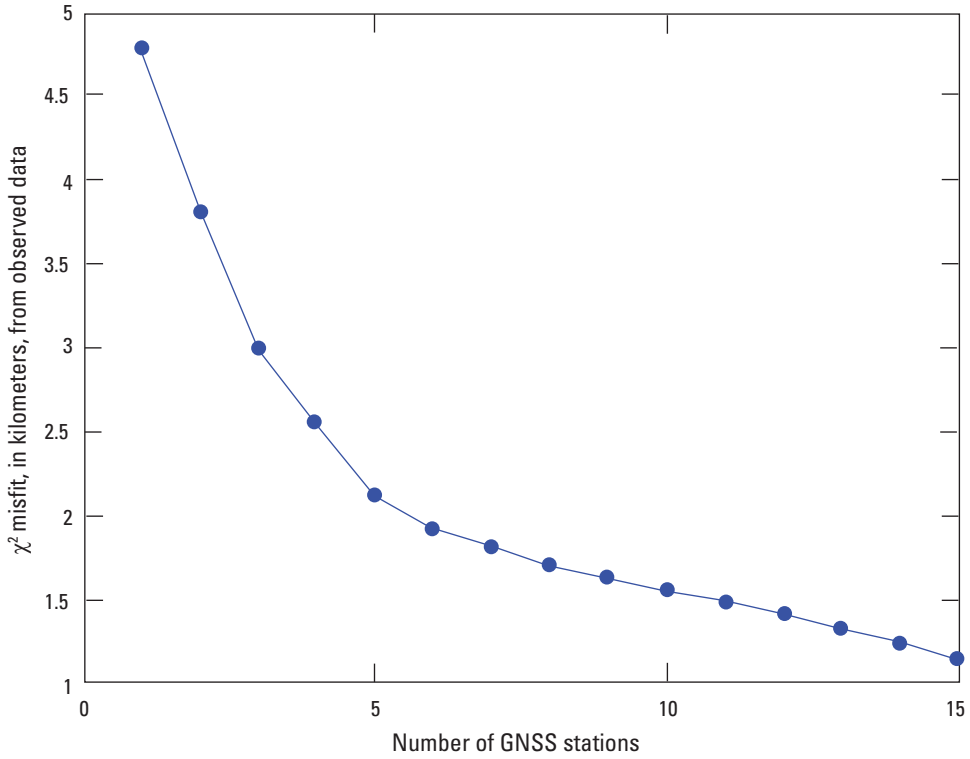

Figure D5. Plot showing the goodness of fit for a modeled magma reservoir determined from a variable number of Global Navigation Satellite System (GNSS) stations. More stations provide better constraints on model parameters (χ^2 represents the combined fitness of four model parameters: depth, two horizontal components of location, and volume change); misfit decreases substantially with more than 5 stations and further improves with 15 stations. The magma reservoir was modeled to be at 2.5 kilometers depth.

Differentiate between Volcanic and Nonvolcanic Ground Deformation

Differentiating volcanic from nonvolcanic (for example, tectonic or hydrologic) surface deformation is crucial to the interpretation of observed displacement patterns and their implications. For example, in 1998, anomalous ground displacements were detected in continuous- and survey-mode GNSS data from Popocatépetl, Mexico (Larson and others, 2004). The surface deformation was associated with transient tectonic slip on the subduction interface, more than 100 km away from the volcano, and therefore presented no significant volcanic hazard. In November 2000, continuous-mode GNSS stations south of Kīlauea's summit moved 2 centimeters closer to the ocean over a period of about 48 hours (Cervelli and others, 2002). The large GNSS network on the Island of Hawai'i enabled scientists to determine that the surface deformation was a result of aseismic fault slip (a small increment of flank collapse) that is sometimes, but not always, directly linked to the ongoing eruption of the volcano, and therefore not indicative of a likely change in the eruption or its impacts (Cervelli and others, 2002; Brooks and others, 2006; Segall and others, 2006; Montgomery-Brown and others, 2015).

At arc volcanoes and other volcanoes in tectonically active regions, significant nonvolcanic deformation is always likely. In addition to volcanic deformation, ground displacements at most volcanoes result from a combination of processes—motion of the volcanic region relative to the stable plate, motion along faults that can be both local and regional (for example, elastic strain resulting from the locked main thrust interface of a subduction zone), and other local processes like geothermal- or groundwater-induced displacements. The tectonic processes commonly can be accounted for by referencing the displacements of the volcano-monitoring stations to sites that are nearby but off the volcano. When no such reference sites are available or when reference sites have failed, plate motion models can be used, but may not be as precise. When the volcanic signal is exceptionally large, the reference sites may be displaced, which can complicate interpretation of the data; however, this situation can be accounted for by explicitly modeling the deformation as being relative to the reference sites. Deformation from local or regional fault motion generally can be compensated for by using data from periods of no volcanic signal or from other regional data. Elastic strain from a locked subduction zone is commonly manifested as approximately arc-normal contraction, can be comparable in magnitude to the volcanic signal, and varies widely in space (for example, Zweck and others, 2002; Dzurisin and others, 2015). Volcanoes commonly lie on or near active upper-crustal faults, motion on which can cause significant ground displacements that may or may not be related to volcanic sources. Numbers of deformation-monitoring instruments, particularly GNSS stations, would ideally be increased for volcanoes on or near major faults to better distinguish magmatic and tectonic processes. Hydrologic signals are usually seasonal in nature and can be distinguished from volcanic signals based on their pattern of occurrence (Langbein, 2017).

Instrumentation

Far-field continuous-mode GNSS stations are needed at distances much farther than the expected depth of the volcanic reservoir to model and remove nonvolcanic deformation signals from local volcano-monitoring networks; the number of stations depends on the size of each volcanic center and the complexity of its tectonic environment. The high-spatial-resolution capability of InSAR can also be exploited to detect fault motion and other nonvolcanic deformation; thus, repeat InSAR analyses would also be performed.

Recommendations

No additional instruments are needed for levels 1 and 2 volcanoes in the absence of unrest. For level 3 volcanoes, it is worth adding additional instrumentation to confirm whether anomalous ground displacements are caused by magmatic phenomena. Five to ten continuous-mode GNSS stations are recommended, of which at least two would ideally be located outside the area of expected deformation (to provide a stable reference) and four within 5–10 km of the deforming source. InSAR measurements would ideally be acquired and analyzed every few years. GNSS surveys would be undertaken every several years to supplement InSAR measurements and data from continuous-mode GNSS stations.

Additional instruments are recommended for level 4 volcanoes to confirm whether anomalous ground displacements are caused by magmatic phenomena and, if it is not magmatic, to identify the cause of the anomalous displacement. We recommend 16 to 20 continuous-mode GNSS stations, of which at least five would be located within 5–10 km of the deforming source and two outside the area of expected deformation (to provide a stable reference). We recommend collecting InSAR measurements annually (summer to summer) or during the summer at volcanoes that are covered by snow during the winter and more frequently at snow-free volcanoes depending on satellite cadence. There would ideally be regular (every few years) GNSS surveys to supplement data from InSAR measurements and continuous-mode GNSS stations. One continuous gravimeter would be placed near the volcano if conditions are appropriate. It should be installed as close as possible to any likely sources of mass change (because the strength of any gravity signal diminishes rapidly with distance) and should be co-located with a continuous-mode GNSS station for elevation control. Repeat gravity surveys would ideally cover the deforming area.

Summary—Recommendations for Level 1–4 Networks

Level 1.—Baseline deformation measurements using InSAR. Establish baseline GNSS and gravity survey networks and repeat surveys occasionally in case future unrest warrants additional data collection.

Level 2.—InSAR images acquired annually or every few years and incorporated into automated processing and analysis. GNSS and gravity surveys repeated every several years (depending on logistics). A single, continuous-mode GNSS station within 5–10 km of the deforming source.

Level 3.—About 5–10 telemetered continuous-mode GNSS stations, of which four are within 5–10 km of the deforming source and one is outside the area of expected deformation. If conditions permit, two to four borehole tiltmeters within 5–10 km of the deforming source. InSAR processing on at least an annual basis, and GNSS and gravity surveys (as appropriate) every several years to supplement data collected from continuously operating stations.

Level 4.—At least 16 continuous-mode GNSS stations, of which at least eight are within 5–10 km of the deforming source and two are outside the area of expected deformation. If conditions are appropriate, four to six borehole tiltmeters within 5–10 km of the deforming source and one continuous gravimeter. Regular InSAR acquisition and processing, including multitemporal approaches as conditions warrant. GNSS and gravity surveys to supplement data collected from continuously operating stations.

References Cited

Aloisi, M., Bonaccorso, A., Gambino, S., Mattia, M., and Puglisi, G., 2003, Etna 2002 eruption imaged from continuous tilt and GPS data: Geophysical Research Letters, v. 30, no. 23, 5 p., https://doi.org/10.1029/2003GL018896.

Amelung, F., Yun, S.-H., Walter, T.R., Segall, P., and Kim, S.W., 2007, Stress control of deep rift intrusion at Mauna Loa volcano, Hawaii: Science, v. 316, no. 5827, p. 1026–1030, https://doi.org/10.1126/science.1140035.

Anderson, K.R., Poland, M.P., Johnson, J.H., and Miklius, A., 2015, Episodic deflation-inflation events at Kīlauea Volcano and implications for the shallow magma system, *in* Carey, R., Cayol, V., Poland, M., and Weis, D., eds., Hawaiian Volcanoes—From source to surface: American Geophysical Union Geophysical Monograph 208, p. 229–250, https://doi.org/10.1002/9781118872079.ch11.

Brandsdóttir, B., Menke, W., Einarsson, P., White, R.S., and Staples, R.K., 1997, Färoe-Iceland Ridge Experiment 2. Crustal structure of the Krafla central volcano: Journal of Geophysical Research, v. 102, no. B4, p. 7867–7886, https://doi.org/10.1029/96JB03799.

Brooks, B.A., Foster, J.H., Bevis, M., Frazer, L.N., Wolfe, C.J., and Behn, M., 2006, Periodic slow earthquakes on the flank of Kīlauea volcano, Hawai'i: Earth and Planetary Science Letters, v. 246, no. 3–4, p. 207–216.

Cervelli, P., Segall, P., Johnson, K., Lisowski, M., and Miklius, A., 2002, Sudden aseismic fault slip on the south flank of Kīlauea Volcano: Nature, v. 415, no. 6875, p. 1014–1018, https://doi.org/10.1038/4151014a.

Cervelli, P.F., Fournier, T., Freymueller, J., and Power, J.A., 2006, Ground deformation associated with the precursory unrest and early phases of the January 2006 eruption of Augustine Volcano, Alaska: Geophysical Research Letters, v. 33, no. 18, https://doi.org/10.1029/2006GL027219.

Chadwick, W.W., Jr., Archuleta, R.J., and Swanson, D.A., 1988, The mechanics of ground deformation precursory to dome-building extrusions at Mount St. Helens, 1981–1982: Journal of Geophysical Research, v. 93, no. B5, p. 4351–4366, https://doi.org/10.1029/JB093iB05p04351.

Chadwick, W.W., Jr., and Swanson, D.A., 1989, Thrust faults and related structures in the crater floor of Mount St. Helens volcano, Washington: Geological Society of America Bulletin, v. 101, no. 12, p. 1507–1519, https://doi.org/10.1130/0016-7606(1989)101<1507:TFARSI>2.3.CO;2.

Delaney, P.T., and McTigue, D.F., 1994, Volume of magma accumulation or withdrawal estimated from surface uplift or subsidence, with application to the 1960 collapse of Kīlauea Volcano: Bulletin of Volcanology, v. 56, no. 6–7, p. 417–424, https://doi.org/10.1007/BF00302823.

Dieterich, J.H., and Decker, R.W., 1975, Finite element modeling of surface deformation associated with volcanism: Journal of Geophysical Research, v. 80, no. 29, p. 4094-4102, https://doi.org/10.1029/JB080i029p04094.

Dzurisin, D., 2000, Volcano geodesy—Challenges and opportunities for the 21st century: Royal Society of London Philosophical Transactions, ser. A, v. 358, no. 1770, p. 1547–1566, https://doi.org/10.1098/rsta.2000.0603.

Dzurisin, D., 2003, A comprehensive approach to monitoring volcano deformation as a window on the eruption cycle: Reviews of Geophysics, v. 41, no. 1, https://doi.org/10.1029/2001RG000107.

Dzurisin, D., 2007, Volcano deformation—New geodetic monitoring techniques: Berlin, Springer-Verlag, 441 p.

Dzurisin, D., Poland, M.P., and Bürgmann, R., 2002, Steady subsidence of Medicine Lake volcano, northern California, revealed by repeated leveling surveys: Journal of Geophysical Research Solid Earth, v. 107, no. B12, https://doi.org/10.1029/2001JB000893.

Dzurisin, D., Moran, S.C., Lisowski, M., Schilling, S.P., Anderson, K.R., and Werner, C., 2015, The 2004–2008 dome-building eruption at Mount St. Helens, Washington—Epilogue: Bulletin of Volcanology, v. 77, no. 10, p. 1–17, https://doi.org/10.1007/s00445-015-0973-4.

Flinders, A.F., Lowenstern, J.B., Coombs, M.L., and Poland, M.P., 2024, Introduction to recommended capabilities and instrumentation for volcano monitoring in the United States, chap. A *of* Flinders, A.F., Lowenstern, J.B., Coombs, M.L., and Poland, M.P., eds., Recommended capabilities and instrumentation for volcano monitoring in the United States: U.S. Geological Survey Scientific Investigations Report 2024–5062–A, 8 p., https://doi.org/10.3133/sir20245062A.

Fournier, T., and Freymueller, J., 2008, Inflation detected at Mount Veniaminof, Alaska, with campaign GPS: Geophysical Research Letters, v. 35, no. 20, https://doi.org/10.1029/2008GL035503.

Grapenthin, R., Freymueller, J.T., and Kaufman, A.M., 2013, Geodetic observations during the 2009 eruption of Redoubt Volcano, Alaska: Journal of Volcanology and Geothermal Research, 259, p. 115–132, https://doi.org/10.1016/j.jvolgeores.2012.04.021.

Hurwitz, S., and Lowenstern, J.B., 2024, Special topic—Boreholes, chap. K *of* Flinders, A.F., Lowenstern, J.B., Coombs, M.L., and Poland, M.P., eds., Recommended capabilities and instrumentation for volcano monitoring in the United States: U.S. Geological Survey Scientific Investigations Report 2024–5062–K, 5 p., https://doi.org/10.3133/sir20245062K.

Iwashita, S., Takahashi, H., Okazaki, N., Miyamura, J., Kasahara, M., Ichiyanagi, M., Takahashi, R., and Nakagawa, M., 2005, Volcanic inflation of Mount Hokkaido-Komagatake, Japan, determined from a dense GPS array: Geophysical Research Letters, v. 32, no. 20, 4 p., https://doi.org/10.1029/2005GL023438.

Iwatsubo, E.Y., Ewert, J.W., and Murray, T.L., 1992, Monitoring radial crack deformation by displacement meters, *in* Ewert, J., and Swanson, D., eds., Monitoring volcanoes—Techniques and strategies used by the staff of the Cascades Volcano Observatory, 1980–90: U.S. Geological Survey Bulletin 1966, p. 95–101.

Kobayashi, T., 2018, Locally distributed ground deformation in an area of potential phreatic eruption, Midagahara volcano, Japan, detected by single-look-based InSAR time series analysis: Journal of Volcanology and Geothermal Research, v. 357, p. 213–223 https://doi.org/10.1016/j.jvolgeores.2018.04.023.

Langbein, J., 2017, Improved efficiency of maximum likelihood analysis of time series with temporally correlated errors: Journal of Geodesy, v. 91, p. 985–994, https://doi.org/10.1007/s00190-017-1002-5.

Larson, K.M., Lowry, A.R., Kostoglodov, V., Hutton, W., Sánchez, O., Hudnut, K., and Suárez, G., 2004, Crustal deformation measurements in Guerrero, Mexico: Journal of Geophysical Research, Solid Earth, v. 109, no. B4, https://doi.org/10.1029/2003JB002843.

Linde, A.T., Agustsson, K., Sacks, I.S., and Stefansson, R., 1993, Mechanism of the 1991 eruptions of Hekla from continuous borehole strain monitoring: Nature, v. 365, no. 6448, p. 737–740, https://doi.org/10.1038/365737a0.

Lipman, P.W., Moore, J.G., and Swanson, D.A., 1981, Bulging of the north flank before the May 18 eruption—Ggeodetic data, *in* Lipman, P.W., and Mullineaux, D.R., eds., The 1980 eruptions of Mount St. Helens, Washington: U.S. Geological Survey Professional Paper 1250, p. 143–156, https://doi.org/10.3133/pp1250.

Miklius, A., and Cervelli, P., 2003, Interaction between Kīlauea and Mauna Loa: Nature, v. 421, no. 229, https://doi.org/10.1038/421229a.

Mogi, K., 1958, Relations between the eruptions of various volcanoes and the deformations of the ground surfaces around them: Earthquake Research Institute Bulletin, v. 36, no. 2, p. 99–134.

Montgomery-Brown, E.K., Poland, M.P., and Miklius, A., 2015, Delicate balance of magmatic-tectonic interaction at Kīlauea Volcano, Hawai‘i, revealed from slow slip events, *in* Carey, R., Cayol, V., Poland, M., and Weis, D., eds., Hawaiian Volcanoes—From source to surface: American Geophysical Union Geophysical Monograph 208, p. 229–250, https://doi.org/10.1002/9781118872079.ch13.

Murray, J.R., and Svarc, J., 2017, Global Positioning System data collection, processing, and analysis conducted by the U.S. Geological Survey Earthquake Hazards Program: Seismological Research Letters, v. 88, no. 3, p. 916–925, https://doi.org/10.1785/0220160204.

Okada, Y., 1985, Surface deformation due to shear and tensile faults in a half-space: Bulletin of the Seismological Society of America, v. 75, no. 4, p. 1135–1154, https://doi.org/10.1785/BSSA0750041135.

Orr, T.R., Dietterich, H.R., and Poland, M.P., 2024, Tracking surface changes caused by volcanic activity, chap. G *of* Flinders, A.F., Lowenstern, J.B., Coombs, M.L., and Poland, M.P., eds., Recommended capabilities and instrumentation for volcano monitoring in the United States: U.S. Geological Survey Scientific Investigations Report 2024–5062–G, 11 p., https://doi.org/10.3133/sir20245062G.

Pagli, C., Sigmundsson, F., Árnadóttir, T., Einarsson, P., and Sturkell, E., 2006, Deflation of the Askja volcanic system—Constraints on the deformation source from combined inversion of satellite radar interferograms and GPS measurements: Journal of Volcanology and Geothermal Research, v. 152, no. 1–2, p. 97–108, https://doi.org/10.1016/j.jvolgeores.2005.09.014.

Peltier, A., Staudacher, T., Catherine, P., Ricard, L.-P., Kowalski, P., and Bachèlery, P., 2006, Subtle precursors of volcanic eruptions at Piton de la Fournaise detected by extensometers: Geophysical Research Letters, v. 33, no. 6, 5 p., https://doi.org/10.1029/2005GL025495.

Pritchard, M.E., and Simons, M., 2004, An InSAR-based survey of volcanic deformation in the central Andes: Geochemistry, Geophysics, Geosystems, v. 5, no. 2, https://doi.org/10.1029/2003GC000610.

Reid, M.E., Sisson, T.W., and Brien, D.L., 2001, Volcano collapse promoted by hydrothermal alteration and edifice shape, Mount Rainier, Washington: Geology, v. 29, no. 9, p. 779–782, https://doi.org/10.1130/0091-7613(2001)029<0779:VCPBHA>2.0.CO;2.

Robertson, R.M., and Kilburn, C.R., 2016, Deformation regime and long-term precursors to eruption at large calderas—Rabaul, Papua New Guinea: Earth and Planetary Science Letters, v. 438, p. 86–94, https://doi.org/10.1016/j.epsl.2016.01.003.

Schaefer, L.N., Di Traglia, F., Chaussard, E., Lu, Z., Nolesini, T., and Casagli, N., 2019, Monitoring volcano slope instability with Synthetic Aperture Radar—A review and new data from Pacaya (Guatemala) and Stromboli (Italy) volcanoes: Earth-Science Reviews, v. 192, p. 236–257, https://doi.org/10.1016/j.earscirev.2019.03.009.

Segall, P., Desmarais, E.K., Shelly, D., Miklius, A., and Cervelli, P., 2006, Earthquakes triggered by silent slip events on Kīlauea Volcano, Hawaii: Nature, v. 442, no. 7098, p. 71–74, https://doi.org/10.1038/nature04938.

Swanson, D.A., Casadevall, T.J., Dzurisin, D., Malone, S.D., Newhall, C.G., and Weaver, C.S., 1983, Predicting eruptions at Mount St. Helens, June 1980 through December 1982: Science, v. 221, no. 4618, p. 1369–1376, https://doi.org/10.1126/science.221.4618.1369.

Varugu, B., and Amelung, F., 2021, Southward growth of Mauna Loa's dike-like magma body driven by topographic stress: Scientific Reports, v. 11, article no. 9816, https://doi.org/10.1038/s41598-021-89203-6.

Wadge, G., Mattioli, G.S., and Herd, R.A., 2006, Ground deformation at Soufrière Hills Volcano, Montserrat during 1998–2000 measured by radar interferometry and GPS: Journal of Volcanology and Geothermal Research, v. 152, no. 1–2, p. 157–173, https://doi.org/10.1016/j.jvolgeores.2005.11.007.

Wicks, C.W., Dzurisin, D., Ingebritsen, S., Thatcher, W., Lu, Z., and Iverson, J., 2002, Magmatic activity beneath the quiescent Three Sisters volcanic center, central Oregon Cascade Range, USA: Geophysical Research Letters, v. 29, no. 7, p. 26-1–26-4, https://doi.org/10.1029/2001GL014205.

Xue, X., and Freymueller, J.T., 2020, A 25-year history of volcano magma supply in the east central Aleutian arc, Alaska: Geophysical Research Letters, v. 47, no. 15, https://doi.org/10.1029/2020GL088388.

Xue, X., Freymueller, J., and Lu, Z., 2020, Modeling the post-eruptive deformation at Okmok based on the GPS and InSAR time series—Changes in the shallow magma storage system: Journal of Geophysical Research, Solid Earth, v. 125, no. 2, https://doi.org/10.1029/2019JB017801.

Yamaoka, K., Geshi, N., Hashimoto, T., Ingebritsen, S.E., and Oikawa, T., 2016, Special issue "The phreatic eruption of Mt. Ontake Volcano in 2014," *in* Yamaoka, K., Ingebritsen, S., Oikawa, T., Hashimoto, T., and Geshi, N., eds., The phreatic eruption of Mt. Ontake Volcano in 2014: Earth, Planets, and Space, v. 68, no. 175, https://doi.org/10.1186/s40623-016-0548-4.

Yun, S., Segall, P., and Zebker, H., 2006, Constraints on magma chamber geometry at Sierra Negra Volcano, Galápagos, based on InSAR observations: Journal of Volcanology and Geothermal Research, v. 150, no. 1–3, p. 232–243, https://doi.org/10.1016/j.jvolgeores.2005.07.009.

Zweck, C., Freymueller, J.T., and Cohen, S.C., 2002, Three-dimensional elastic dislocation modeling of the postseismic response to the 1964 Alaska earthquake: Journal of Geophysical Research, Solid Earth, v. 107, no. B4, 12 p., https://doi.org/10.1029/2001JB000409.

Moffett Field Publishing Service Center, California
Manuscript approved July 10, 2024
Edited by Linda Rogers and Monica Erdman
Layout and design by Cory Hurd

ISSN 2328-031X (print)
ISSN 2328-0328 (online)
https://doi.org/10.3133/sir20245062D